THE JOURNAL OF PHYSICAL CHEMISTRY C

Article

pubs.acs.org/JPCC

Oxidation, Destruction, and Persistence of Multilayer Dimethyl Methylphosphonate Films during Exposure to O(^{3}P) Atomic Oxygen

Grant G. Langlois, Rebecca S. Thompson, Wenxin Li, and S. J. Sibener*

The James Franck Institute and Department of Chemistry The University of Chicago, 929 E. 57th Street, Chicago, Illinois 60637, United States

ABSTRACT: We present work detailing the oxidative reactivity of the nerve agent simulant dimethyl methylphosphonate (DMMP) with atomic oxygen using time-resolved *in situ* reflection−absorption infrared spectroscopy (RAIRS) and X-ray photoelectron spectroscopy (XPS). When exposed to a supersonic beam containing O(^{3}P) with average translational energy of 0.12 eV, thermally annealed DMMP films (less than 50 layers) on single-crystal Au(111) are observed to react, likely *via* hydrogen abstraction, and followed by various secondary reactions with resultant hydroxyl and DMMP-derived radicals. This reaction is accompanied by the appearance of hydrogen bonding interactions with the DMMP phosphoryl (P═O) groups on the film surface, and it is also observed to result in both a loss of carbon and an uptake of oxygen by the film. These trends, when considered with the additional thermal stability of reaction products left on the surface, suggest that the mechanism entails reaction with DMMP methyl groups and the formation of various polymeric species; the presence of these polymers hinders continuous, effective destruction for films thicker than roughly ten layers. This work has specific implications for the implementation of plasma-based and oxidative decontamination methods based upon an improved fundamental understanding of the chemistry of the important class of phosphoryl containing molecules.

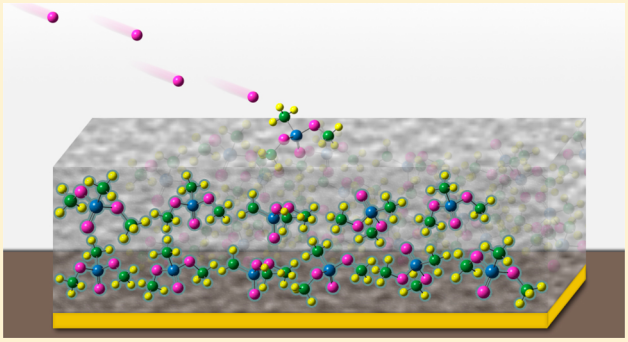

INTRODUCTION

The 1993 Chemical Weapons Convention prohibits the creation and stockpiling of chemical weapons, yet these dangerous compounds remain a critical social and environmental threat.[1] Whether decontaminating attack sites or destroying unused chemical weapon stores, there is a great risk to both civilians and military personnel if these agents' surface interactions are not properly understood; any new destruction strategy must, in addition to removing the toxic agent, account for volatile byproducts, secondary contamination, and waste disposal.[2] As such, it is critical to have a comprehensive grasp of the agents' destruction pathways and mechanisms, persistence, and potential redispersal on a myriad of representative environmental and industrial materials.

The surface interactions of nerve agents and their simulants have been investigated thoroughly on a number of surfaces to date, including metals,[3−7] metal oxides,[4,8−19] nanoparticle assemblies,[20−22] and other thin films;[23−26] complementary theoretical analyses have also been published for many of these systems.[27−34] Notably, many of these materials (particularly metal oxides) have demonstrated significant catalytic activity in the decomposition of surface adsorbed dimethyl methylphosphonate (DMMP), a common nerve agent simulant. While effective, active site poisoning often limits the practicality of these methods on a large scale. Furthermore, these oxide materials are often difficult to reactivate once poisoned.[12,14] To overcome these limitations and establish continuous decomposition activity, Mitchell et al. have explored the reaction of DMMP and ozone on alumina-supported iron oxide and manganese oxide. Measurements of the resultant CO and CO_2 production revealed higher catalytic activity in the presence of ozone, due to the formation of reactive atomic oxygen species resulting from ozone's decomposition on the oxide surface.[35,36]

Additional nerve agent decontamination strategies involve exposure to atmospheric pressure plasma sources.[37−41] While many current decontamination methods rely on complete incineration at high temperatures[42−44] or corrosive wet chemicals (*i.e.*, bleach), use of these plasmas provides a nondestructive, environmentally safe alternative that precludes mass storage and long exposure times.[2,41] Like the aforementioned continuous decomposition studies, the effectiveness of this method is also linked to the presence of both ozone and atomic oxygen in the plasmas.[39] In addition to clarifying the basic mechanisms underlying some of these destruction techniques, the results of this study may also shed light on the known flame-retarding properties of organophosphate compounds.[45,46]

Informed by recent theoretical work on gas-phase reactivity between DMMP and O(^{3}P),[47,48] we present a detailed picture of the oxidative destruction of multilayer DMMP films and

Received: June 10, 2016
Revised: July 1, 2016
Published: July 20, 2016

DOI: 10.1021/acs.jpcc.6b05880
J. Phys. Chem. C 2016, 120, 16863−16870

elucidate the mechanistic role of atomic oxygen in its destruction. Reflection−absorption infrared spectroscopy (RAIRS) and X-ray photoelectron spectroscopy (XPS) were used to demonstrate that DMMP reacts upon exposure to $O(^3P)$ under ultrahigh vacuum (UHV) conditions, and that the reaction likely generates additional reactive species on the surface. Furthermore, we present clear evidence that overall reactivity decays upon continued exposure, and results in formation of additional byproducts possessing greater thermal stability on the surface than the original DMMP. Reactive oxygen species have been shown to be important in the destruction of nerve agents and their simulants in applications ranging from preventative surface treatments to post-contamination remediation. The findings contained herein have direct implications for understanding the fate of dispersed agents subject to naturally occurring oxygen species and better inform development of safe and effective decontamination techniques.[49,50]

EXPERIMENTAL SECTION

All experiments were conducted in a molecular beam scattering instrument described in detail in a previous publication.[51] The instrument is comprised of a triply differentially pumped molecular beamline attached to a chamber under UHV. In the chamber, a single crystal Au(111) sample is exposed to the beam and the subsequent interfacial dynamics are monitored in real time *via in situ* RAIRS and XPS.

DMMP was deposited on single-crystal Au(111) in the chamber *via* a directed doser located approximately two inches from the crystal front. RAIR spectra, fit to Gaussian peaks on cubic baselines, were used to characterize the surface and extent of reactivity. Spectra were obtained with a Nicolet 6700 infrared spectrometer; *p*-polarized IR radiation was reflected from the Au(111) substrate at a 75° incident angle and collected in a liquid-nitrogen-cooled MCT/A detector. Spectra were averaged over 300 scans at 4 cm^{-1} resolution, using sputtered/annealed Au(111) as the background reference signal. A representative spectrum of a DMMP film is shown in Figure 1. The intense P−O−C and P═O modes, highlighted in the figure's inset, are most frequently referenced herein, with observed peak positions and assignments informed by and consistent with the literature.[6,10,11,16,26] For all experiments involving reaction of DMMP with $O(^3P)$, the surface temperature was held at 155 K during dosing, where DMMP desorption is observed to be negligible. After dosing, the films were annealed at 175 K until desired thicknesses were reached.

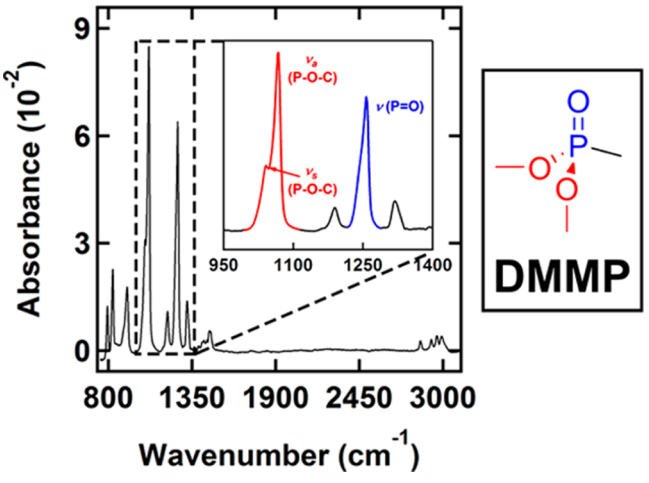

Figure 1. RAIR spectrum of 40-layer thick DMMP film on single-crystal Au(111). Notable signals discussed throughout text include the P−O−C (red, 1041 and 1066 cm^{-1}) and P═O (blue, ∼1240−1260 cm^{-1}) stretching modes; these are highlighted in the DMMP molecule and spectrum inset.

A series of isothermal desorption experiments allowed for initial DMMP film thickness quantification *via* RAIRS (Figure 2). DMMP films were subjected to desorption at surface

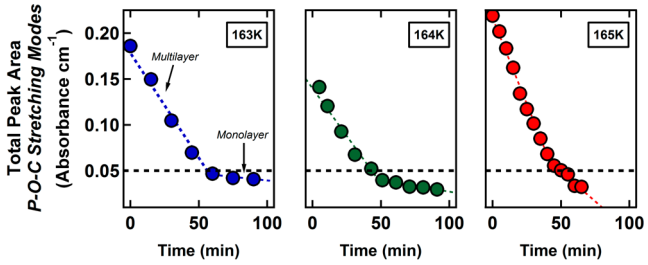

Figure 2. Isothermal desorption of DMMP films allows for quantification of initial film thicknesses *via* integrated P−O−C signal intensity. Transitioning from multilayer to monolayer desorption exhibits a marked decrease in desorption rate; the value where this occurs correlates with the infrared intensity of a single layer of DMMP.

temperatures ranging from 163 to 165 K, and the integrated areas of the P−O−C stretching modes were tracked as a function of time. Total integrated peak intensity is observed to decay linearly at two different rates, corresponding to a difference in multilayer and monolayer desorption rates, respectively.[52] As displayed in each panel of Figure 2, the spectroscopic signature of the monolayer is determined from the point at which the rate abruptly changes. Using our experimental setup, one layer of DMMP corresponds to a total integrated P−O−C peak intensity of 0.05 absorbance units cm^{-1}. Initial film thicknesses reaching upward of 50 layers were quantified using this procedure, given that peak line shapes remained consistent with continued DMMP exposure across this range.

A previously described radio frequency plasma source generated supersonic expansions containing atomic oxygen.[53] A gas mixture of 5% O_2 in neon flowed through a water-cooled quartz nozzle, with 35−60% of the O_2 subsequently dissociating to $O(^3P)$ in the high temperature plasma localized at the end of the nozzle. We note that under certain conditions, this type of discharge source may also produce trace concentrations of O^+ ions and $O(^1D)$, both of which exhibit different reactivity in comparison to $O(^3P)$, such as insertion as opposed to abstraction. However, the presence of a 2000 V/cm deflecting field region in our instrument for the incident beam filters out any ionic species downstream, and the RF power and gas pressure used in the current study (100 W and 75 Torr, respectively) are both significantly lower than the conditions typically used when one seeks to intentionally produce $O(^1D)$ beams for reactive studies.[53−55]

Time-of-flight experiments quantified $O(^3P)$ translational energy and flux. Total $O(^3P)$ flux was determined from the integrated peak areas of time-of-flight spectra obtained for the O_2 component of the expansion as measured by an in-line quadrupole mass spectrometer (QMS) calibrated to the flux of a neat O_2 beam.[56] The pressure rise in the chamber for the neat beam was measured with a nude Bayard-Alpert ion gauge, and the flux was calculated using this pressure rise, the chamber

DOI: 10.1021/acs.jpcc.6b05880
J. Phys. Chem. C 2016, 120, 16863−16870

pumping speed, the relative sensitivity of the gauge to O_2,[57,58] and the spot size on the Au(111) crystal. The $O(^3P)$ flux is related to the O_2 flux through the O_2 dissociation percentage. Typical values for the average translational energy and flux of $O(^3P)$ from the beam impinging at normal incidence are, respectively, 0.12 eV and 5×10^{16} atoms cm^{-2} s^{-1}. Beam energy widths are approximately 0.06 eV.

During XPS experiments, X-rays from an Al Kα (1486.6 eV) X-ray source operating at 10 kV and 20 mA irradiated the sample at a 45° incident angle. Spectra in the C(1s), O(1s), and Au(4f) regions were obtained using a double pass cylindrical mirror analyzer (PHI model 15-255G) with a 50 eV pass energy and 0.4 eV step size, with peaks fit in the same manner as that used in RAIRS analyses. The binding energy scale was calibrated in reference to the intense pair of Au(4f) peaks at 87.63 and 83.95 eV.[59]

RESULTS AND DISCUSSION

Spectral Assignment and Film Reactivity. A number of spectral changes are clearly observed upon exposing DMMP films to $O(^3P)$. Figure 3 depicts, chronologically, changes in the methoxy group signals (1041 and 1066 cm^{-1}) of the film as a function of total $O(^3P)$ exposure. While the peak locations, consistent with reported values for the symmetric and antisymmetric P−O−C stretches,[11,23,24] remain unchanged, both peaks are observed to decrease in intensity in Figure 3a. Given the multilayer character of the films studied, this behavior cannot be attributed to a change in average orientation of these groups and is instead ascribed to reactive destruction. In contrast, the total integrated intensity of the P═O stretching modes of a given film P═O (~1240−1260 cm^{-1}) does not exhibit the same behavior. As seen in Figure 3b, total P═O intensity is left unchanged by extended $O(^3P)$ exposure.

Spectra highlighting the individual peaks that comprise the P═O stretching region are depicted in Figure 4a. P═O peak positions are highly sensitive to coordination environment, whether *via* hydrogen bonding or direct physisorption to surface metal (Lewis acid) sites.[6,15,19,23,60] While the overall intensity in this region is unchanged during exposure, there are a number of significant changes in the peak shape. Prior to $O(^3P)$ exposure, the P═O stretch can be deconvoluted into separate signals at 1249 and 1258 cm^{-1}. These peak locations are consistent with recorded values for DMMP adsorbed on unreactive, nonhydroxylated surfaces.[23−25] Exposure to $O(^3P)$ causes the intensity of the 1258 cm^{-1} peak to decrease, replaced by a new signal at 1214 cm^{-1}, highlighted in Figure 4b. This shift is consistent with DMMP coordination with hydroxlyated metal oxides or other hydroxyl-terminated surfaces, in which the P═O stretch is weakened and red-shifted by the formation of one or two hydrogen bonds.[11,12,23] Further corroborating this assignment is a separate control experiment performed where a DMMP monolayer was deposited on a 50- to 60-layer

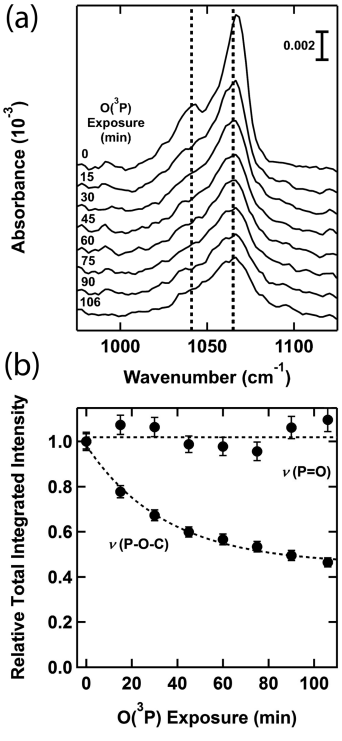

Figure 3. (a) RAIRS signal in the P−O−C region of a 6-layer thick DMMP film obtained during exposure to a molecular beam containing 0.12 eV $O(^3P)$ (flux = 2.9×10^{16} cm^{-2} s^{-1}); total intensity is observed to decay as a function of total $O(^3P)$ exposure. (b) Total integrated RAIR peak intensities normalized to their initial values show that, unlike the P−O−C signal intensity, the total P═O intensity is left unchanged by $O(^3P)$ exposure. Dotted lines are drawn with intent to guide the eye. Error bars, where visible, indicate one standard deviation with respect to the peak fitting.

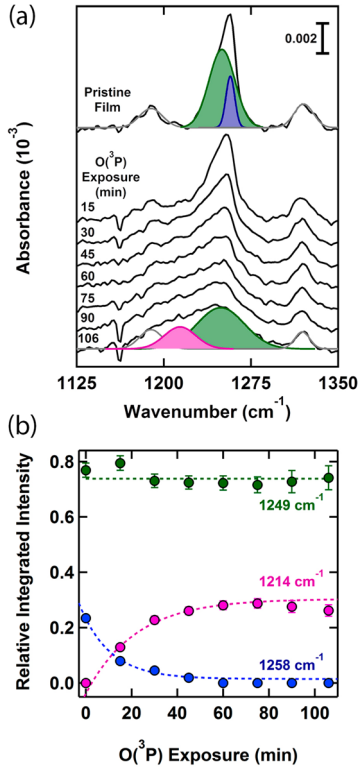

Figure 4. (a) P═O signals throughout exposure are deconvoluted into contributions from three signals at 1258, 1249, and 1214 cm^{-1}. Individual peaks are shown to illustrate the decay of the 1258 cm^{-1} peak coupled with the emergence of the 1214 cm^{-1} peak during exposure ($O(^3P)$ flux = 2.9×10^{16} cm^{-2} s^{-1}). (b) Corresponding integrated areas of the P═O stretching peaks demonstrate that the 1249 cm^{-1} peak is unaffected by $O(^3P)$ exposure, while 1258 and 1214 cm^{-1} peaks exchange intensity. Dotted lines are drawn to guide the eye. Error bars, where visible, indicate one standard deviation with respect to the peak fitting.

DOI: 10.1021/acs.jpcc.6b05880
J. Phys. Chem. C 2016, 120, 16863−16870

thick amorphous solid water film at 125 K. Detailed in Figure 5, a comparison of the P═O signals of one DMMP layer

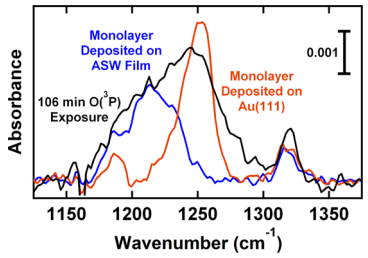

Figure 5. Appearance of the 1214 cm^{-1} peak in the spectrum of a six-layer DMMP film exposed to $O(^3P)$ for 106 min (black, 2.9×10^{16} atoms cm^{-2} s^{-1}) is compared to the spectra of a DMMP monolayer deposited on clean Au(111) (gold) versus on thick amorphous water ice (blue). This peak's position is consistent with the observed red-shift of the monolayer deposited on water ice, indicative of new hydrogen bonding interactions with the phosphoryl group of DMMP as a result of $O(^3P)$-induced reactivity.

deposited on Au(111) versus water ice shows a red shift identical to that observed upon exposure of a multilayer film to $O(^3P)$. Finally, this shift is also consistent with DMMP solvation in the liquid phase.[25,61]

Importantly, only one of the two initial P═O peaks is impacted by $O(^3P)$ exposure; the 1249 cm^{-1} peak remains essentially unchanged (Figure 4b) except for some broadening. In order to explain this disparity, it is important to identify the two initial peaks. One possible explanation is conformational; DMMP is reported to have at least two low energy conformers in both the solid and gas phase.[6,32,62−65] Electronic structure calculations predict that the P═O peaks for the two lowest-energy conformers in the gas phase could be as little as 2 cm^{-1} apart.[65] On the other hand, a splitting of 20 cm^{-1} between conformers has been interpreted from FTIR spectra of solid- and liquid-phase DMMP.[63] Our observed splitting of ∼9 cm^{-1} is within this range, but the lack of agreement complicates definitive assignment. A supplemental explanation may involve the organization of DMMP in the solid film. It has been suggested that spectroscopic signals associated with DMMP aggregates appear between 1240 and 1250 cm^{-1}.[63] A consequence of DMMP aggregates would likely be two general molecular environments. The reactive 1258 cm^{-1} peak could potentially represent molecules at the boundaries of such aggregates, while the 1249 cm^{-1} peak, mostly unchanging during exposure to $O(^3P)$, could correspond to DMMP molecules within the interior of these aggregates. This latter argument is supported by spectroscopically observing DMMP growth, in which the two peak intensities were tracked as DMMP was deposited. The 1258/1249 integrated intensity ratio remains constant from one layer and beyond, eliminating the possibility that the 1258 cm^{-1} peak corresponds simply to DMMP at the vacuum- or substrate−film interfaces.

Product Formation. Evidence of partial DMMP film destruction is given by the decrease in intensity of the P−O−C stretching modes; this is corroborated by consistent decreases in the C−H stretching mode region below 3000 cm^{-1} upon $O(^3P)$ exposure. At the film thicknesses studied the IR intensity for these C−H modes are weak and preclude more detailed spectral analysis. We support the proposed mechanism by citing recent theoretical calculations for collision dynamics between DMMP and $O(^3P)$ in the gas phase, the results of which indicate that hydrogen abstraction is the most energetically accessible reaction channel. The calculated upper limit for the gas phase barriers are 0.14 and 0.36 eV for abstraction from the methoxy or methyl groups, respectively.[47,48] These barriers are, however, likely lower in the solid phase due to formation of longer-lived collision complexes in the film. Furthermore, experimental evidence suggests that reactions between $O(^3P)$ and organic or hydrocarbon-based films does proceed largely through an abstraction mechanism.[66−68] In the present study, hydrogen abstraction would naturally yield hydroxyl radicals as products:

$$O{=}P(CH_3)(OCH_3)_2 + O(^3P) \rightarrow O{=}P(CH_3)(OCH_3)(OCH_2)^{\bullet} + {}^{\bullet}OH \quad (1)$$

These reactive species can be expected to undergo further reactions within the film. For example:

$$O{=}P(CH_3)(OCH_3)(OCH_2)^{\bullet} \rightarrow O{=}P(CH_3)(OCH_3)^{\bullet} + OCH_2 \quad (2)$$

Reaction 2, in particular, could help explain the observed methoxy group loss during exposure. Figure 6 contains a plot of

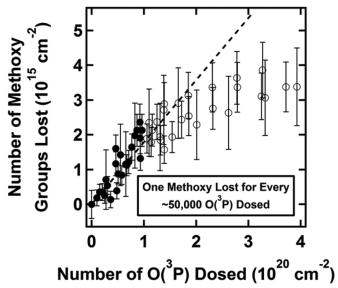

Figure 6. Aggregated data for all experiments showing methoxy group loss from DMMP as a function of $O(^3P)$ exposure. A linear fit to the data early in the exposure (solid circles) shows that one methoxy group reacts for approximately every 50 000 $O(^3P)$ dosed onto the surface. See text for details regarding the estimation of the ordinate data from the infrared spectra.

all aggregated data collected, arranged to show methoxy group loss as a function of $O(^3P)$ exposure. The ordinate axis values estimate that a DMMP monolayer is comprised of 6×10^{14} molecules/cm^2 *via* its gas phase geometry[5] and take into account that there are two methoxy groups per DMMP molecule. The observed reactivity does not follow simple first- or even half-order kinetics with respect to $O(^3P)$ exposure; the observed behavior is likely the product of numerous reactions contributing to the observed spectroscopic changes. We can, however, consider the initial reactivity to get a sense for the initial reaction probability. A linear fit to the data early in the exposure (solid circles in Figure 6) shows that in the first stages of reaction, a methoxy group is lost for roughly every 50 000 $O(^3P)$ dosed onto the surface. If direct reaction occurs, this rather low probability could be a result of only a fraction of the incident $O(^3P)$ having sufficient energy to overcome the barrier. Otherwise, after collision and exchange of energy with the film, $O(^3P)$ would then have to diffuse both along and through the vacuum-film interface to encounter a methyl group.

Changes in the P═O region of the spectra during reaction also suggest formation of hydroxyl species, given that conversion of signal from 1258 to 1214 cm^{-1} is consistent

DOI: 10.1021/acs.jpcc.6b05880
J. Phys. Chem. C 2016, 120, 16863−16870

with "solvation" of phosphoryl oxygens *via* hydrogen bonding.[25,61] It is worth noting that phosphoryl stretching modes of organophosphorus compounds are also influenced by inductive effects from other functional groups attached to the central phosphorus atom.[69] However, all reaction routes considered in the aforementioned theoretical studies—hydrogen abstraction, hydrogen elimination, and methyl elimination—would not result in a redshift of this mode.

XPS data displayed in Figure 7 suggest that in addition to carbon loss, possibly as gaseous CO or CO_2,[36] the reaction

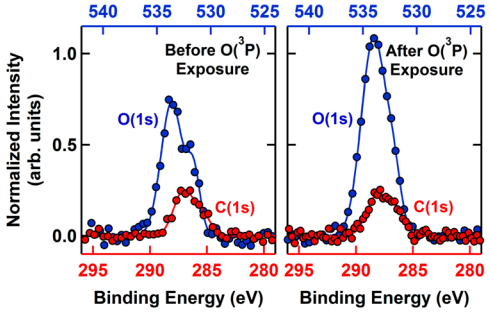

Figure 7. Representative XPS data comparing DMMP films as deposited and after exposure to $O(^3P)$ show that the N_O/N_C ratio increases as a result of oxygen uptake by the film. To emphasize this effect, the data are scaled such that the carbon 1s peak areas are equivalent; this accounts for the fact that some carbon is also lost as gaseous species during reaction.

results in incorporation of oxygen into the film. Comparison of C(1s) and O(1s) signals between a reacted film and a pristine film, normalized to respective film thicknesses, shows a definitive increase in the relative N_O/N_C ratio at the surface. Reactions with $O(^3P)$ and OH radicals would leave radical intermediates that could also react with nondissociated O_2 present in the molecular beam.[70] Thus, there are at least three sources of oxygen resulting from exposure to the beam that are likely contributing to the observed uptake of oxygen in the DMMP film upon beam exposure. These various uptake pathways are further supported by the O(1s) peak shapes before and after $O(^3P)$ exposure. On a pristine DMMP film, the O(1s) spectrum is comprised of two signals, attributed to the methoxy and phosphoryl oxygens in DMMP. After $O(^3P)$ exposure, however, the O(1s) signal is no longer so neatly deconvoluted into distinct oxygen chemical environments.

A slight IR signal increase near 3300 cm^{-1}, indicative of hydroxyl group formation, is observed during exposure to $O(^3P)$, but the rate of growth is convoluted with the small amount of background water deposition expected under our conditions ($(4-8) \times 10^{-11}$ Torr based on readings from a residual gas analyzer). It is important to note, however, that the observed P═O shift does not take place without exposure to $O(^3P)$. DMMP films left in the chamber for periods of time equal to that of an experiment (2 h on average) show no spectroscopic change except for slight growth in the OH region amounting to less than half a layer of water (one layer = 1.07×10^{15} H_2O molecules[71]). Moreover, the films remain unchanged when exposed to a pure neon plasma and a mixture of 5% O_2 in helium (no plasma; approximation of O_2 with higher translational energy present in O_2/Ne plasma). We thus conclude that these changes are initiated by reaction of the film with $O(^3P)$ and cannot simply be attributed to background water sticking to the vacuum-film interface.

The remaining P−O−C and P═O stretching mode signals of films having an initial thickness below ten layers (e.g., Figures 3 and 4) are clearly broadened with respect to the pristine peaks, indicating disordering. The close spatial proximity of radical intermediates could promote formation of polymeric species on the surface, which have been reported at least once in the literature under related circumstances.[38] To test this hypothesis and monitor the thermal stability of the reaction products on the surface *in situ*, isothermal desorption experiments were performed by increasing the surface temperature in a stepwise fashion and obtaining RAIR spectra at each temperature. The surface temperature was ramped up from 155 K in 10 K increments at 1 K/s and held constant during the duration of an IR scan (roughly 3 min) between each step. Results were compared to a pristine film subjected to identical treatment, and a summary is given in Figure 8. From these data

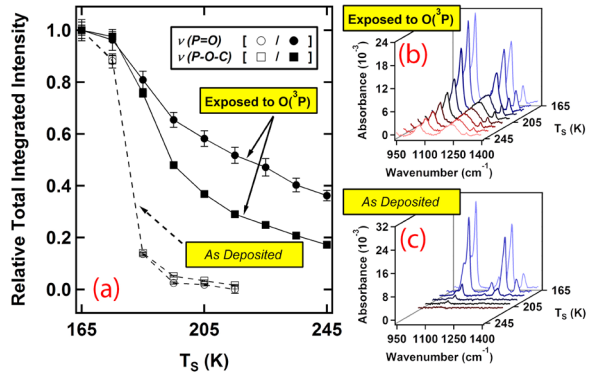

Figure 8. (a) Stepped isothermal desorption experiments (see text for details) show that after reaction of a DMMP film with $O(^3P)$, a portion of the film exhibits substantially greater thermal stability on the substrate. The P−O−C and P═O modes still exhibit appreciable intensity in spectra of reacted films collected at surfaces temperatures above ∼195 K as compared to the pristine film as deposited on Au(111). The respective spectra are given in waterfall plots in (b) and (c).

we can conclude that *a reacted film's thermal stability on the Au(111) substrate differs dramatically from that of the pristine film.* Whereas the total P−O−C and P═O integrated intensities of the pristine film are effectively zero by the time the surface temperature reaches 195 K, these peaks are readily observable at 245 K and beyond for the reacted film. Indeed, the most dramatic changes occur during the ramp from 185 to 195 K for a pristine DMMP film, as emphasized in Figure 9a. This behavior is mirrored in the reacted DMMP film shown in Figure 9b, where the nonreacted DMMP molecules freely desorb, leaving behind the polymeric species and therefore some intensity at 1249 cm^{-1}. The new signal at 1214 cm^{-1} stays essentially constant during the ramp (Figure 9c) and therefore directly corresponds to the presence of the new, more thermally stable polymeric product. Reacted films further show a clear difference in desorption kinetics between the P−O−C and P═O groups (Figure 8a), and we propose that the combination of increased surface energy and trapped oxygen species induces additional secondary reactions within the film during thermal annealing. These reactions further destroy DMMP methoxy groups, leading to a faster observed rate of decay in those particular infrared signals.

Hydrogen-bonded phosphoryl groups (1214 cm^{-1}), as mentioned previously, are products of the reactions taking

DOI: 10.1021/acs.jpcc.6b05880
J. Phys. Chem. C 2016, 120, 16863−16870

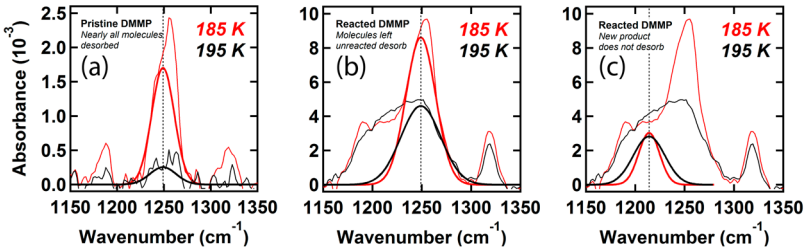

Figure 9. Behavior of the deconvoluted P═O spectroscopic signals of DMMP during isothermal desorption of films both pristine and exposed to $O(^3P)$. The majority of a pristine DMMP film desorbs on the ramp from 185 to 195 K, as shown in (a). This behavior, shown in (b), is mirrored in a reacted DMMP film, where the nonreacted DMMP is free to desorb, leaving behind the polymeric species, and therefore some intensity at 1249 cm^{-1}. Given that its intensity stays essentially constant during the ramp, the new signal at 1214 cm^{-1} is therefore directly related to formation of the new, more thermally stable polymeric product, shown in (c).

place on the surface, and based on the desorption evidence they are likely part of a hydroxylated polymerized species that has significantly greater thermal stability on the surface. In Figure 10, product formation resulting from reactions of $O(^3P)$ with 6,

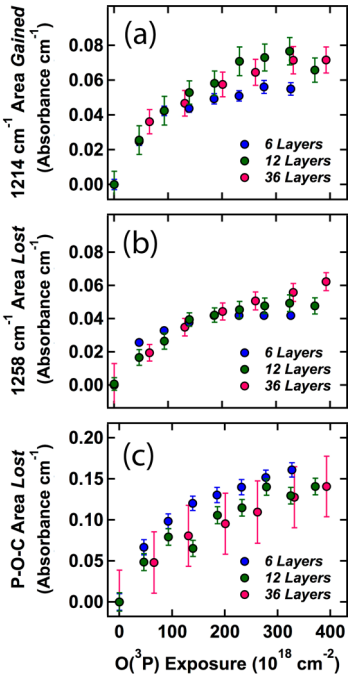

Figure 10. RAIR spectra obtained for 6, 12, and 36 layer DMMP films during exposure to $O(^3P)$ suggest that reaction probability decreases as exposure continues but does not follow half- or first-order kinetics. Panels depict (a) intensity gained in the 1214 cm^{-1} peak, (b) intensity lost from the 1258 cm^{-1} peak, and (c) total intensity lost from the P–O–C stretching modes. Overlap of the data asserts that reactivity is independent of initial film thickness and originates at the vacuum-film interface. Error bars, where visible, indicate one standard deviation with respect to the peak fitting.

12, and 36 layer DMMP films begins to terminate at similar absolute signal intensities on all films studied. If the reaction begins at the vacuum–film interface and progresses layer-by-layer into the bulk DMMP, this trend suggests a limit to the penetration depth of the reactive species. Given substantial film thickness, a fraction of the DMMP—presumably underneath—*is unchanged under our reaction conditions and is left free to desorb from the surface normally upon heating.* Coupled with the decay kinetics mentioned previously, reaction energetics presented here seem to preclude the ability for $O(^3P)$ to erode thicker DMMP films all the way down to the substrate; we hypothesize that the polymeric overlayer formed hinders continued destruction. It is therefore likely that the effectiveness of surface DMMP decontamination through use of atmospheric plasmas cited in the literature[37−41] is facilitated by thermal desorption or sputtering in addition to reactivity with oxygen species.

CONCLUSION

The oxidative reactivity of solid multilayer DMMP by $O(^3P)$ has been characterized using time-resolved RAIRS and complemented by XPS. Our analysis suggests that destruction is initiated *via* hydrogen abstraction from methyl or methoxy groups. In turn, resultant hydroxyl and DMMP radical intermediates formed subsequently react with surrounding DMMP molecules and also potentially with additional O_2 present in the beam under our conditions. While XPS confirms that some carbon is lost from the surface, it also shows oxygen incorporation within the film resulting from continued exposure. At 155 K, 0.12 eV $O(^3P)$ atoms do not destroy thicker ($\gtrsim$10 layers) DMMP films all the way down to the substrate on which they are deposited. We propose that the radical side-reactions initiated by $O(^3P)$ under our experimental conditions yield hydroxylated polymers whose presence hinders continuous destruction of a significant fraction of thicker DMMP films. Despite this observed resistance, unreacted DMMP can freely desorb from the Au(111) surface upon thermal annealing, leaving the polymeric products behind.

These findings better inform the exploration of oxidative decontamination and destructive methods for nerve agents. Based on our observations, the observed efficacy of atmospheric plasma decontamination treatments possibly stems from a combination of the presence of $O(^3P)$, local heating, and sputtering. Additionally, the oxidation-induced formation of a thermally stable polymeric coating may supplement the understanding of these compounds' known flame retarding properties. To this end, our work naturally leads to further investigation into the role of local heating on the destruction of DMMP on surfaces both reactive and inert. Moreover, fruitful extension of this work would involve examining reactivity on model environmental surfaces such as SAMs, ices, and biopolymers, leading to better understanding regarding the limits of effective decontamination following dispersal in a chemical/biological warfare environment.

AUTHOR INFORMATION

Corresponding Author

*E-mail: s-sibener@uchicago.edu.

DOI: 10.1021/acs.jpcc.6b05880
J. Phys. Chem. C 2016, 120, 16863−16870

Notes

The authors declare no competing financial interest.

■ ACKNOWLEDGMENTS

This work was sponsored by the Defense Threat Reduction Agency (DTRA) under Grant HDTRA1-11-1-0001. Additional infrastructure support was provided by the NSF-Materials Research Science and Engineering Center at The University of Chicago, Grant No. NSF-DMR-14-20709. Insightful discussions with K. D. Gibson are gratefully acknowledged.

■ REFERENCES

(1) Bothe, M. A. The Chemical Weapons Convention: A General Overview. In *The New Chemical Weapons Convention: Implementation and Prospects*; Bothe, M., Natalino Ronzitti, A. R., Ed.; Kluwer Law International: Cambridge, MA, 1999; p 600.

(2) Kim, K.; Tsay, O. G.; Atwood, D. A.; Churchill, D. G. Destruction and Detection of Chemical Warfare Agents. *Chem. Rev.* **2011**, *111*, 5345−5403.

(3) Davies, P. R.; Newton, N. G. The Chemisorption of Organophosphorus Compounds at an Al(111) Surface. *Appl. Surf. Sci.* **2001**, *181*, 296−306.

(4) Ekerdt, J. G.; Klabunde, K. J.; Shapley, J. R.; White, J. M.; Yates, J. T. Surface Chemistry of Organophosphorus Compunds. *J. Phys. Chem.* **1988**, *92*, 6182−6188.

(5) Hegde, R. I.; Greenlief, C. M.; White, J. M. Surface Chemistry of Dimethyl Methylphosphonate on Rh(100). *J. Phys. Chem.* **1985**, *89*, 2886−2891.

(6) Henderson, M. A.; White, J. M. Adsorption and Decomposition of Dimethyl Methylphosphonate on Platinum(111). *J. Am. Chem. Soc.* **1988**, *110*, 6939−1947.

(7) Smentkowski, V. S.; Hagans, P.; Yates, J. T. Study of the Catalytic Destruction of Dimethyl Methylphosphonate: Oxidation over Mo(110). *J. Phys. Chem.* **1988**, *92*, 6351−6357.

(8) Chen, D. A.; Ratliff, J. S.; Hu, X.; Gordon, W. O.; Senanayake, S. D.; Mullins, D. R. Dimethyl Methylphosphonate Decomposition on Fully Oxidized and Partially Reduced Ceria Thin Films. *Surf. Sci.* **2010**, *604*, 574−587.

(9) Davis, E. D.; Gordon, W. O.; Wilmsmeyer, A. R.; Troya, D.; Morris, J. R. Chemical Warfare Agent Surface Adsorption: Hydrogen Bonding of Sarin and Soman to Amorphous Silica. *J. Phys. Chem. Lett.* **2014**, *5*, 1393−1399.

(10) Kim, C.; Lad, R.; Tripp, C. Interaction of Organophosphorous Compounds with TiO_2 and WO_3 Surfaces Probed by Vibrational Spectroscopy. *Sens. Actuators, B* **2001**, *76*, 442−448.

(11) Mitchell, M. B.; Sheinker, V. N.; Mintz, E. A. Adsorption and Decomposition of Dimethyl Methylphosphonate on Metal Oxides. *J. Phys. Chem. B* **1997**, *101*, 11192−11203.

(12) Panayotov, D. A.; Morris, J. R. Uptake of a Chemical Warfare Agent Simulant (DMMP) on TiO_2: Reactive Adsorption and Active Site Poisoning. *Langmuir* **2009**, *25*, 3652−3658.

(13) Panayotov, D. A.; Morris, J. R. Thermal Decomposition of a Chemical Warfare Agent Simulant (DMMP) on TiO_2: Adsorbate Reactions with Lattice Oxygen as Studied by Infrared Spectroscopy. *J. Phys. Chem. C* **2009**, *113*, 15684−15691.

(14) Segal, S. R.; Cao, L.; Suib, S. L.; Tang, X.; Satyapal, S. Thermal Decomposition of Dimethyl Methylphosphonate over Manganese Oxide Catalysts. *J. Catal.* **2001**, *198*, 66−76.

(15) Wilmsmeyer, A. R.; Gordon, W. O.; Davis, E. D.; Troya, D.; Mantooth, B. A.; Lalain, T. A.; Morris, J. R. Infrared Spectra and Binding Energies of Chemical Warfare Nerve Agent Simulants on the Surface of Amorphous Silica. *J. Phys. Chem. C* **2013**, *117*, 15685−15697.

(16) Wilmsmeyer, A. R.; Uzarski, J.; Barrie, P. J.; Morris, J. R. Interactions and Binding Energies of Dimethyl Methylphosphonate and Dimethyl Chlorophosphate with Amorphous Silica. *Langmuir* **2012**, *28*, 10962−10967.

(17) Gordon, W. O.; Tissue, B. M.; Morris, J. R. Adsorption and Decomposition of Dimethyl Methylphosphonate on Y_2O_3 Nanoparticles. *J. Phys. Chem. C* **2007**, *111*, 3233−3240.

(18) Bermudez, V. M. Investigation of the Interaction of γ-Al_2O_3 with Aqueous Solutions of Dimethyl Methylphosphonate Using Infrared Multiple Internal Reflection Spectroscopy. *Langmuir* **2013**, *29*, 1483−1489.

(19) Bermudez, V. M. Effect of Humidity on the Interaction of Dimethyl Methylphosphonate (DMMP) Vapor with SiO_2 and Al_2O_3 Surfaces, Studied Using Infrared Attenuated Total Reflection Spectroscopy. *Langmuir* **2010**, *26*, 18144−18154.

(20) Li, Y.; Klabunde, K. J. Nanoscale Metal Oxide Particles as Chemical Reagents. Destructive Adsorption of a Chemical Agent Simulant, Dimethyl Methylphosphonate, on Heat-Treated Magnesium Oxide. *Langmuir* **1991**, *7*, 1388−1393.

(21) Panayotov, D. A.; Morris, J. R. Catalytic Degradation of a Chemical Warfare Agent Simulant: Reaction Mechanisms on TiO_2-Supported Au Nanoparticles. *J. Phys. Chem. C* **2008**, *112*, 7496−7502.

(22) Mattsson, A.; Lejon, C.; Štengl, V.; Bakardjieva, S.; Opluštil, F.; Andersson, P. O.; Österlund, L. Photodegradation of DMMP and CEES on Zirconium Doped Titania Nanoparticles. *Appl. Catal., B* **2009**, *92*, 401−410.

(23) Bertilsson, L.; Engquist, I.; Liedberg, B. Interaction of Dimethyl Methylphosphonate with Alkanethiolate Monolayers Studied by Temperature-Programmed Desorption and Infrared Spectroscopy. *J. Phys. Chem. B* **1997**, *101*, 6021−6027.

(24) Bertilsson, L.; Potje-Kamloth, K.; Liess, H.-D.; Liedberg, B. On the Adsorption of Dimethyl Methylphosphonate on Self-Assembled Alkanethiolate Monolayers: Influence of Humidity. *Langmuir* **1999**, *15*, 1128−1135.

(25) Bertilsson, L.; Potje-Kamloth, K.; Lieβ, H.-D. Molecular Interaction of DMMP and Water Vapor with Mixed Self-Assembled Monolayers Studied by IR Spectroscopy and SAW Devices. *Thin Solid Films* **1996**, *284*−*285*, 882−887.

(26) Ferguson-McPherson, M. K.; Low, E. R.; Esker, A. R.; Morris, J. R. Sorption of Dimethyl Methylphosphonate within Langmuir-Blodgett Films of Trisilanolphenyl Polyhedral Oligomeric Silsesquioxane. *J. Phys. Chem. B* **2005**, *109*, 18914−18920.

(27) Bermudez, V. M. Quantum-Chemical Study of the Adsorption of DMMP and Sarin on γ-Al_2O_3. *J. Phys. Chem. C* **2007**, *111*, 3719−3728.

(28) Bermudez, V. M. Computational Study of the Adsorption of Trichlorophosphate, Dimethyl Methylphosphonate, and Sarin on Amorphous SiO_2. *J. Phys. Chem. C* **2007**, *111*, 9314−9323.

(29) Bermudez, V. M. Computational Study of Environmental Effects in the Adsorption of DMMP, Sarin, and VX on γ-Al_2O_3: Photolysis and Surface Hydroxylation. *J. Phys. Chem. C* **2009**, *113*, 1917−1930.

(30) Quenneville, J.; Taylor, R. S.; Van Duin, A. C. T. Reactive Molecular Dynamics Studies of DMMP Adsorption and Reactivity on Amorphous Silica Surfaces. *J. Phys. Chem. C* **2010**, *114*, 18894−18902.

(31) Yang, L.; Taylor, R.; de Jong, W. A.; Hase, W. L. A Model DMMP/TiO_2 (110) Intermolecular Potential Energy Function Developed from Ab Initio Calculations. *J. Phys. Chem. C* **2011**, *115*, 12403−12413.

(32) Troya, D.; Edwards, A. C.; Morris, J. R. Theoretical Study of the Adsorption of Organophosphorous Compounds to Models of a Silica Surface. *J. Phys. Chem. C* **2013**, *117*, 14625−14634.

(33) Taylor, D. E.; Runge, K.; Cory, M. G.; Burns, D. S.; Vasey, J. L.; Hearn, J. D.; Griffith, K.; Henley, M. V. Surface Binding of Organophosphates on Silica: Comparing Experiment and Theory. *J. Phys. Chem. C* **2013**, *117*, 2699−2708.

(34) Michalkova, A.; Ilchenko, M.; Gorb, L.; Leszczynski, J. Theoretical Study of the Adsorption and Decomposition of Sarin on Magnesium Oxide. *J. Phys. Chem. B* **2004**, *108*, 5294−5303.

(35) Mitchell, M. B.; Sheinker, V. N.; Cox, W. W. Room Temperature Reaction of Ozone and Dimethyl Methylphosphonate (DMMP) on Alumina-Supported Iron Oxide. *J. Phys. Chem. C* **2007**, *111*, 9417−9426.

DOI: 10.1021/acs.jpcc.6b05880
J. Phys. Chem. C 2016, 120, 16863−16870

(36) Mitchell, M. B.; Sheinker, V. N.; Cox, W. W., Jr.; Hardcastle, K. Sustained Room Temperature Decomposition of Dimethyl Methylphosphonate (DMMP) by O_3 on Alumina-Supported MnO_x. *J. Phys. Chem. C* **2011**, *115*, 11514−11524.
(37) Li, Z.; Li, Y.; Cao, P.; Zhao, H. Surface Decontamination of Chemical Agent Surrogates Using an Atmospheric Pressure Air Flow Plasma Jet. *Plasma Sci. Technol.* **2013**, *15*, 696−701.
(38) Moeller, T. M.; Alexander, M. L.; Engelhard, M. H.; Gaspar, D. J.; Luna, M. L.; Irving, P. M. Surface Decontamination of Simulated Chemical Warfare Agents Using a Nonequilibrium Plasma With Off-Gas Monitoring. *IEEE Trans. Plasma Sci.* **2002**, *30*, 1454−1459.
(39) Kim, D. B.; Gweon, B.; Moon, S. Y.; Choe, W. Decontamination of the Chemical Warfare Agent Simulant Dimethyl Methylphosphonate by Means of Large-Area Low-Temperature Atmospheric Pressure Plasma. *Curr. Appl. Phys.* **2009**, *9*, 1093−1096.
(40) Zhu, W.-C.; Wang, B.-R.; Xi, H.-L.; Pu, Y.-K. Decontamination of VX Surrogate Malathion by Atmospheric Pressure Radio-Frequency Plasma Jet. *Plasma Chem. Plasma Process.* **2010**, *30*, 381−389.
(41) Herrmann, H. W.; Henins, I.; Park, J.; Selwyn, G. S. Decontamination of Chemical and Biological Warfare (CBW) Agents Using an Atmospheric Pressure Plasma Jet (APPJ). *Phys. Plasmas* **1999**, *6*, 2284−2289.
(42) Zegers, E. J. P.; Fisher, E. M. Gas-Phase Pyrolysis of Diisopropyl Methylphosphonate. *Combust. Flame* **1998**, *115*, 230−240.
(43) Korobeinichev, O. P.; Ilyin, S. B.; Shvartsberg, V. M.; Chernov, A. A. The Destruction Chemistry of Organophosphorus Compounds in flames—I: Quantitative Determination of Final Phosphorus-Containing Species in Hydrogen-Oxygen Flames. *Combust. Flame* **1999**, *118*, 718−726.
(44) Glaude, P. A.; Melius, C.; Pitz, W. J.; Westbrook, C. K. Detailed Chemical Kinetic Reaction Mechanisms for Incineration of Organophosphorus and Fluoroorganophosphorus Compounds. *Proc. Combust. Inst.* **2002**, *29*, 2469−2476.
(45) Liang, S.; Hemberger, P.; Neisius, N. M.; Bodi, A.; Grützmacher, H.; Levalois-Grützmacher, J.; Gaan, S. Elucidating the Thermal Decomposition of Dimethyl Methylphosphonate by Vacuum Ultraviolet (VUV) Photoionization: Pathways to the PO Radical, a Key Species in Flame-Retardant Mechanisms. *Chem. - Eur. J.* **2015**, *21*, 1073−1080.
(46) Korobeinichev, O. P.; Shvartsberg, V. M.; Shmakov, A. G.; Bolshova, T. A.; Jayaweera, T. M.; Melius, C. F.; Pitz, W. J.; Westbrook, C. K.; Curran, H. Flame Inhibition by Phosphorus-Containing Compounds in Lean and Rich Propane Flames. *Proc. Combust. Inst.* **2005**, *30*, 2353−2360.
(47) Conforti, P. F.; Braunstein, M.; Dodd, J. A. Energetics and Dynamics of the Reactions of $O(^3P)$ with Dimethyl Methylphosphonate and Sarin. *J. Phys. Chem. A* **2009**, *113*, 13752−13761.
(48) Conforti, P. F.; Braunstein, M.; Stearns, J. A.; Dodd, J. A. Collision Dynamics of $O(^3P)$ + DMMP Using a Specific Reaction Parameters Potential Form. *J. Phys. Chem. A* **2012**, *116*, 2506−2518.
(49) Davisson, M.; Love, A.; Vance, A.; Reynolds, J. *Environmental Fate of Organophosphorus Compounds Related to Chemical Weapons*; Lawrence Livermore National Laboratory: Livermore, CA, 2005.
(50) Fitch, J. P.; Raber, E.; Imbro, D. R. Technology Challenges in Responding to Biological or Chemical Attacks in the Civilian Sector. *Science* **2003**, *302*, 1350−1354.
(51) Gibson, K. D.; Killelea, D. R.; Yuan, H.; Becker, J. S.; Sibener, S. J. Determination of the Sticking Coefficient and Scattering Dynamics of Water on Ice Using Molecular Beam Techniques. *J. Chem. Phys.* **2011**, *134*, 034703.
(52) Gibson, K. D.; Sibener, S. J. Scattering Dynamics, Survival, and Dispersal of Dimethyl Methylphosphonate Interacting with the Surface of Multilayer Graphene. *J. Phys. Chem. A* **2016**, DOI: 10.1021/acs.jpca.5b12419.
(53) Sibener, S. J.; Buss, R. J.; Ng, C. Y.; Lee, Y. T. Development of a Supersonic $O(^3P_J)$, $O(^1D_2)$ Atomic Oxygen Nozzle Beam Source. *Rev. Sci. Instrum.* **1980**, *51*, 167−182.
(54) Alagia, M.; Aquilanti, V.; Ascenzi, D.; Balucani, N.; Cappelletti, D.; Cartechini, L.; Casavecchia, P.; Pirani, F.; Sanchini, G.; Volpi, G. G. Magnetic Analysis of Supersonic Beams of Atomic Oxygen, Nitrogen, and Chlorine Generated from a Radio-Frequency Discharge. *Isr. J. Chem.* **1997**, *37* (4), 329−342.
(55) Casavecchia, P.; Balucani, N.; Volpi, G. G. Reactive Scattering of $O(^3P, ^1)D)$, $Cl(^2P)$ and OH Radicals. In *The Chemical Dynamics and Kinetics of Small Radicals*; Wagner, A., Liu, K., Eds.; World Scientific Publishing Company: Singapore, 1996; pp 365−426.
(56) Gibson, K. D.; Langlois, G. G.; Li, W.; Killelea, D. R.; Sibener, S. J. Molecular Interactions with Ice: Molecular Embedding, Adsorption, Detection, and Release. *J. Chem. Phys.* **2014**, *141*, 18C514.
(57) Itikawa, Y. Cross Sections for Electron Collisions with Nitrogen Molecules. *J. Phys. Chem. Ref. Data* **2006**, *35*, 31−53.
(58) Itikawa, Y. Cross Sections for Electron Collisions with Oxygen Molecules. *J. Phys. Chem. Ref. Data* **2009**, *38*, 1−20.
(59) Crist, V. B. Handbooks of Monochromatic XPS Spectra Volume 1 - The Elements and Native Oxides. *Handb. Elem. Nativ. Oxides* **1999**, *1*, 1−43.
(60) Templeton, M.; Weinberg, W. H. Decomposition of Phosphonate Esters Adsorbed on Aluminum Oxide. *J. Am. Chem. Soc.* **1985**, *107*, 774−779.
(61) Eaton, G.; Harris, L.; Patel, K.; Symons, M. C. R. Infrared and Nuclear Magnetic Resonance Spectroscopic Studies on the Solvation of Trimethylphosphate and Dimethylphosphonate. *J. Chem. Soc., Faraday Trans.* **1992**, *88*, 3527−3531.
(62) Herman, M. A.; Van Der Veken, B. J.; Barnes, A. J. Vibrational Studies on Conformational Equilibrium in Dimethylmethylphosphonate and Methyldimethylphosphinate. *J. Mol. Struct.* **1983**, *99*, 197−206.
(63) Lomax, S.; Barnes, A. J.; Van Der Veken, B. J. Conformational Behaviour of Dimethylmethylphosphonate and Methyldimethylphosphinate Studied by Infrared Spectroscopy in Low-Temperature Matrices. *J. Mol. Struct.* **1983**, *99*, 137−145.
(64) Vishnyakov, A.; Neimark, A. V. Molecular Model of Dimethylmethylphosphonate and Its Interactions with Water. *J. Phys. Chem. A* **2004**, *108*, 1435−1439.
(65) Cuisset, A.; Mouret, G.; Pirali, O.; Roy, P.; Cazier, F.; Nouali, H.; Demaison, J. Gas-Phase Vibrational Spectroscopy and Ab Initio Study of Organophosphorus Compounds: Discrimination between Species and Conformers. *J. Phys. Chem. B* **2008**, *112*, 12516−12525.
(66) Garton, D. J.; Minton, T. K.; Alagia, M.; Balucani, N.; Casavecchia, P.; Gualberto Volpi, G.; Egitto, F. D.; Matienzo, L. J.; Liston, E. M.; Hartney, M. A.; et al. Reactive Scattering of Ground-State and Electronically Excited Oxygen Atoms on a Liquid Hydrocarbon Surface. *Faraday Discuss.* **1997**, *108*, 387−399.
(67) Garton, D. J.; Minton, T. K.; Alagia, M.; Balucani, N.; Casavecchia, P.; Gualberto Volpi, G. Comparative Dynamics of $Cl(^2P)$ and $O(^3P)$ Interactions with a Hydrocarbon Surface. *J. Chem. Phys.* **2000**, *112*, 5975−5984.
(68) Paz, Y.; Trakhtenberg, S.; Naaman, R. Reaction between $O(^3P)$ and Organized Organic Thin-Films. *J. Phys. Chem.* **1994**, *98*, 13517−13523.
(69) Thomas, L. C. *Interpretation of the Infrared Spectra of Organophosphorus Compounds*; Heyden & Son Ltd.: London, 1974.
(70) Aschmann, S. M.; Tuazon, E. C.; Atkinson, R. Atmospheric Chemistry of Diethyl Methylphosphonate, Diethyl Ethylphosphonate, and Triethyl Phosphate. *J. Phys. Chem. A* **2005**, *109*, 2282−2291.
(71) Henderson, M. A. The Interaction of Water with Solid Surfaces: Fundamental Aspects Revisited. *Surf. Sci. Rep.* **2002**, *46*, 1−308.

DOI: 10.1021/acs.jpcc.6b05880
J. Phys. Chem. C 2016, 120, 16863−16870